ADVANCED FUNCTIONAL MATERIALS
www.afm-journal.de

www.MaterialsViews.com

3D Hierarchical Co_3O_4 Twin-Spheres with an Urchin-Like Structure: Large-Scale Synthesis, Multistep-Splitting Growth, and Electrochemical Pseudocapacitors

Yuanhua Xiao, Shaojun Liu, Feng Li, Aiqin Zhang, Jihong Zhao, Shaoming Fang, and Dianzhen Jia**

Novel, 3D hierarchical Co_3O_4 twin-spheres with an urchin-like structure are produced successfully on the large scale for the first time by a solvothermal synthesis of cobalt carbonate hydroxide hydrate, $Co(CO_3)_{0.5}(OH)\cdot 0.11H_2O$, and its subsequent calcination. The morphology of the precursor, which dominates the structure of the final product, evolves from nanorods to sheaf-like bundles, to flower-like structures, to dumbbell-like particles, and eventually to twin-spheres, accompanying a prolonged reaction time. A multistep-splitting growth mechanism is proposed to understand the formation of the 3D hierarchical twin-spheres of the precursor, based on the time effect on the morphologies of the precursor. The 3D hierarchical Co_3O_4 twin-spheres are further used as electrode materials to fabricate supercapacitors with high specific capacitances of 781, 754, 700, 670, and 611 F g^{-1} at current densities of 0.5, 1, 2, 4, and 8 A g^{-1}, respectively. The devices also show high charge-discharge reversibility with an efficiency of 97.8% after cycling 1000 times at a current density of 4 A g^{-1}.

1. Introduction

Due to the fact that the functionalities of materials can be tuned efficiently through manipulating their structures, diverse strategies have been developed successfully to produce materials with well-defined structures. In order to improve further the performances of energy storage devices such as supercapacitors, it is highly desirable to fabricate materials with not only a large specific-surface area for high activity, but also a stable 3D hierarchical structure with excellent ability for electron transportation and negligible ion-diffusion time.[1–6] These two crucial characters of electrode materials, however, often conflict to some extent and consequently cannot always be satisfied at the same time. Extensive research concerned with improving the performance of supercapacitors have therefore concentrated on optimizing the microstructures of electrode materials, especially 3D hierarchical structures, to take the advantages both of the high stability of bulk materials and the activity of nanosized materials.[3,7–21] Li rechargeable batteries[12,22] and supercapacitors[19] with improved performances have been designed and fabricated to tackle the globally emerging challenges in energy security in recent years.

As novel energy storage devices developed from Leyden Jar invented in 1745, supercapacitors have been paid less attention than batteries until recent years, because of a further understanding of the mechanism of their excellent specific capacitances, and the fabrication of novel electrode materials with tunable compositions and microstructures.[3,7–21] Hydrous RuO_2 supercapacitors,[20,21,23] for instance, exhibit high specific capacitances, as high as 1580 F g^{-1}, while their practical applications are limited due to their high cost. Low-cost transition metal oxide materials including Fe_2O_3,[24] MnO_2,[14,25–27] WO_3/MoO_3,[15,28] Co_3O_4,[29–54] and their composites[7,8,16,17] have thus been investigated extensively in recent years to explore alternative and effective pathways to access electrode materials with controlled nanostructures and construct novel energy-storage devices with excellent performances.

Because of the relatively low environmental footprint, low-cost, and the high specific capacitance of 3560 F g^{-1} in theory, cobalt cobaltite (Co_3O_4) is one of the promising materials for the design and fabrication of supercapacitors.[29–54] Based on the mechanism that dictates the performance of supercapacitors, it is critical to control the structures of electrode materials to improve the kinetics of electron transportion and ion diffusion.[1,3–6] Co_3O_4 nanocrystals with diverse structures including ultralayered structures,[37,55] nanosheets,[30] nanowires,[33,49] nanoparticles,[29] and nanotubes[45] have been synthesized successfully and utilized as building blocks to construct supercapacitors recently. However, it is still rare to find reports concerned with the growth and energy storage functionalities of 3D hierarchical Co_3O_4 nanostructures.

Y. Xiao, S. Liu, Prof. F. Li, A. Zhang,
Dr. J. Zhao, Dr. S. Fang
College of Materials and Chemical Engineering
State Laboratory of Surface and
Interface Science and Technology
Zhengzhou University of Light Industry
Zhengzhou 450002, P. R. China
E-mail: lifeng696@yahoo.com; fengli@zzuli.edu.cn
Prof. F. Li, Prof. D. Jia
Institute of Applied Chemistry
Xinjiang University
Urumqi 830046, Xinjiang P. R. China
E-mail: jdz0991@gmail.com

DOI: 10.1002/adfm.201200519

Herein, we report the large-scale synthesis and excellent electrochemical performances of 3D hierarchical Co_3O_4 twin-spheres with an urchin-like structure, for the first time. The novel 3D nanoarchitectures were produced by calcining the precursor, cobalt carbonate hydroxide hydrate, $Co(CO_3)_{0.5}(OH)\cdot 0.11H_2O$, with a 3D hierarchical twin-spherical structure, synthesized by a solvothermal method. The as-prepared twin-spheres are composed of 1D Co_3O_4 nanochains with a granular structure, generated by the oxidation and decomposition of single-crystalline nanoneedles of the precursor. Moreover, based on the effect of the reaction time on the morphology of the precursor, a multistep-splitting growth mechanism is proposed to understand the formation of the 3D hierarchical nanostructures. The electrochemical performances of the 3D hierarchical Co_3O_4 twin-spheres were further investigated carefully. It was found that supercapacitors constructed with the materials exhibited high specific capacitances of 781, 754, 700, 670, and 611 F g^{-1} at current densities of 0.5, 1, 2, 4, and 8 A g^{-1}, respectively. The devices also showed a high reversibility with an efficiency of 97.8% after cycling 1000 times at a current density of 4 A g^{-1}. The excellent electrochemical performances of the supercapacitors can be attributed to the novel 3D hierarchical structure of the Co_3O_4 twin-spheres.

2. Results and Discussion

The red powders of the precursor were characterized using X-ray diffraction (XRD) to verify their structure. All of the diffraction peaks, as shown in **Figure 1**a, could be indexed as orthorhombic cobalt carbonate hydroxide hydrate, $Co(CO_3)_{0.5}(OH)\cdot 0.11H_2O$ (JCPDS card No. 48-0083). The morphology of the precursor could be revealed by field-emission scanning electron microscopy (FE-SEM) (Figure 1b) and transmission electron microscopy (TEM) (inset in Figure 1c) observations. We successfully obtained 3D hierarchical twin-spheres with an urchin-like structure with diameters ranging from 10 to 15 μm. The TEM image shown in Figure 1c shows segments disassembled from the 3D hierarchical twin-spheres by ultrasonic treatment. Precursor nanoneedles, with a smooth surface and a plate-like shape, and with a width of 5–150 nm were generated. The high-resolution TEM (HR-TEM) image (Figure 1d) of the segments shows fringes perpendicular to the axis of the nanoneedle, which clearly indicates the single-crystalline nature of the precursor nanoneedles. The measured lattice spacing of 0.293 nm corresponds to the interlayer spacing of the (300) planes of the $Co(CO_3)_{0.5}(OH)\cdot 0.11H_2O$. The results indicate that 1D nanoneedles grew along the [100] direction. In addition, the corresponding, well-ordered dot pattern of the selected-area electron diffraction (SAED) (insert in Figure 1d) again shows the single-crystalline nature of the orthorhombic $Co(CO_3)_{0.5}(OH)\cdot 0.11H_2O$ nanoneedles.

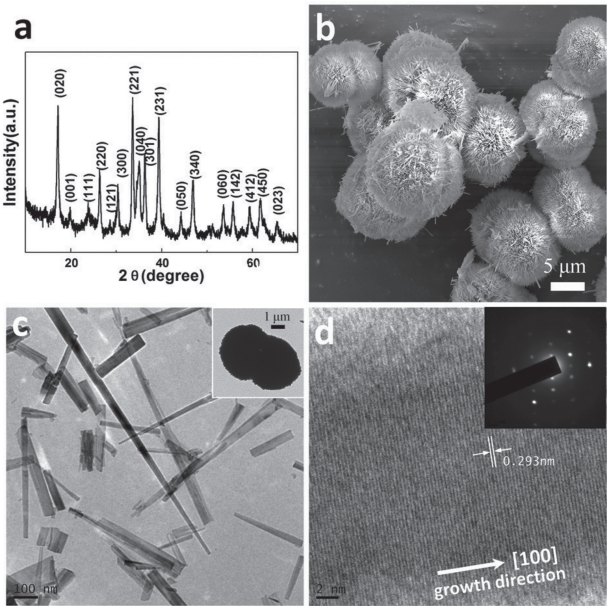

Figure 1. a) XRD pattern of cobalt carbonate hydroxide hydrate. b) FE-SEM image of the precusor. c) TEM image of the nanoneedles disassembled from the precusor by ultrasound treatment. The inset shows a low-magnification TEM image of one twin-sphere of the precursor. d) HR-TEM image and SAED pattern (inset) from one of the precursor nanoneedles.

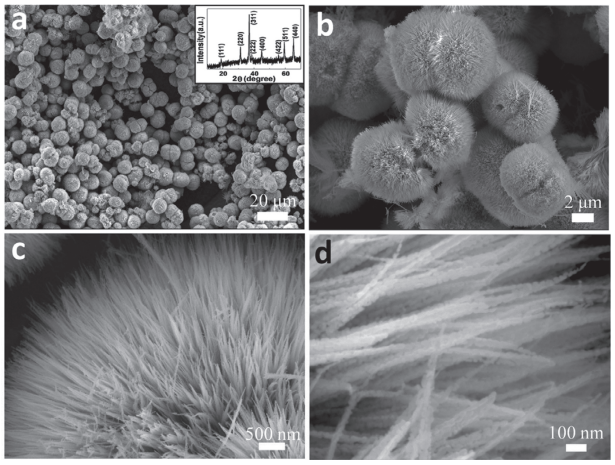

Figure 2. a) Low-magnification FE-SEM image of 3D hierarchical Co_3O_4 twin-spheres after annealing at 300 °C for 2 h. The inset shows the corresponding XRD pattern of the materials. b–d) High-magnification FE-SEM images of the 3D hierarchical Co_3O_4 twin-spheres.

Figure 2 presents FE-SEM images and the XRD pattern of the final Co_3O_4 products prepared by annealing the precursor at 300 °C for 2 h. The XRD pattern of the as-prepared sample (inset in Figure 2a) consists of seven diffraction peaks attributed to the (111), (220), (311), (222), (400), (422), (511), and (440) planes of the cubic Co_3O_4 phase (JCPDS card No. 42-1467), respectively. There were no diffraction peaks from any other impurities, which indicates the high purity of the cobalt cobaltite products. The low-magnification FE-SEM image of the as-prepared sample (Figure 2a) shows that the final products inherited the 3D hierarchical structure of the precursor. 3D Co_3O_4 twin-spheres with an urchin-like structure, with diameters ranging from 10 to 15 μm, were successfully produced on a large scale. The high-magnification FE-SEM images of the as-prepared materials (Figure 2b–d) show that the hierarchical

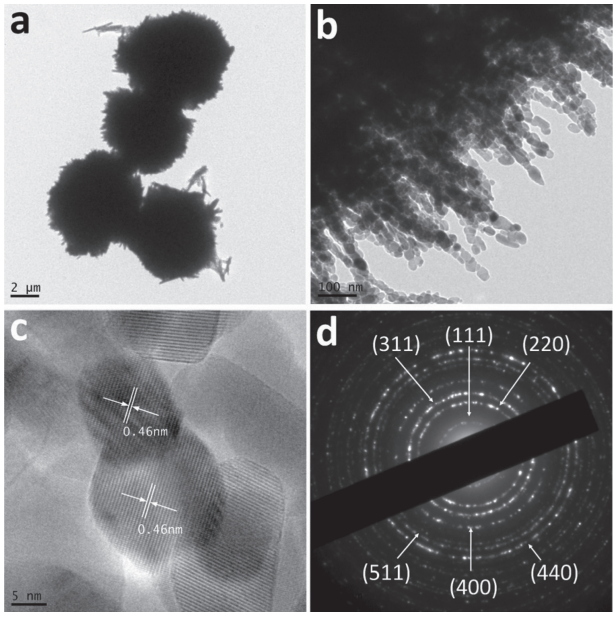

Figure 3. a,b) TEM images of the 3D hierarchical Co_3O_4 twin-spheres after annealing at 300 °C for 2 h. c,d) HR-TEM image (c) and SAED pattern (d) of Co_3O_4 nanochains consisting of Co_3O_4 nanoparticles.

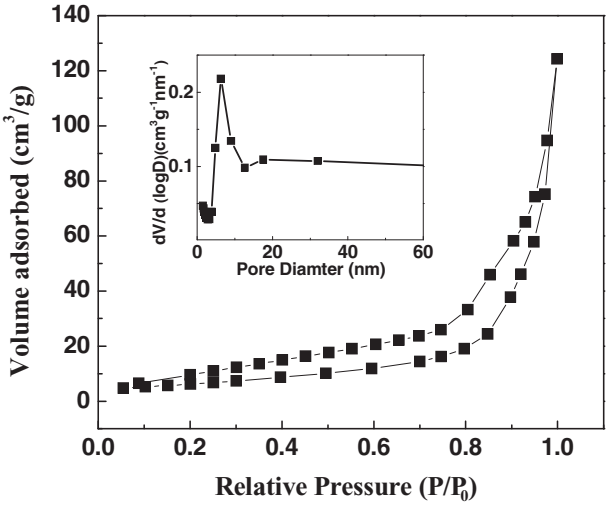

Figure 4. Typical nitrogen-adsorption-desorption isotherm and pore-size-distribution curve (inset) of the 3D hierarchical Co_3O_4 twin-spheres.

Co_3O_4 twin-spheres were composed of 1D nanochains with rough surfaces, which grew radically to form urchin-like structures from their centers. The Co_3O_4 nanochains were produced from the oxidation and decomposition of the single-crystalline nanoneedles of the precursor, which induced the formation of the granular structure. The hierarchical Co_3O_4 twin-spheres with their urchin-like structure may offer not only 3D networks for electron transportation, but also spaces critical for ion diffusion, which dominate the energy-storage performance of supercapacitors.

The structures of the Co_3O_4 twin-spheres were further characterized by TEM and SAED. **Figure 3**a presents a TEM image of two Co_3O_4 twin-spheres at low magnification to show the whole view of the 3D hierarchical structure. The enlarged TEM image of one such sphere, as shown in Figure 3b, further confirms that the 3D hierarchical nanostructures were composed of 1D nanochains consisting of nanoparticles with diameter ranging from 5–30 nm. The nanoparticles were fused together to form 1D nanochains. The crystal structure of the materials was further characterized by HR-TEM observations (Figure 3c). The *d*-spacings of approximately 0.46 nm correspond to the (111) planes of cubic Co_3O_4, while the lattices as shown in Figure 3c were oriented to different directions randomly. These results indicate the high crystallinity of the nanoparticles and the polycrystalline feature of the nanochains, in contrast to the single-crystalline structure of the precursor nanoneedles. The SAED pattern (Figure 3d) of the twin-spheres further confirms their polycrystalline feature. The six most-distinct concentric diffraction rings from the center could be assigned to the (111), (220), (311), (400), (511), and (440) planes of cubic Co_3O_4, which agrees well with the results obtained from the XRD pattern (inset in Figure 2a).

The porous structure of the 3D hierarchical Co_3O_4 nanoarchitectures was further evaluated by Brunauer–Emmett-Teller (BET) N_2-adsorption-desorption analysis. **Figure 4** shows the adsorption-desorption isotherm and the corresponding Barrett-Joyner-Halenda (BJH) pore-size-distribution plot (inset in Figure 4) of the 3D hierarchical twin-spheres. According to the International Union of Pure and Applied Chemistry (IUPAC) classification, the loop observed was ascribed as a type-H3 loop, indicating the existence of abundant pores 2 to 50 nm in diameter. While the size and shape of the pores were not uniform, most of them were around 6.30 nm in diameter (pore volume: 0.19 $cm^3\ g^{-1}$) and the average pore diameter was approximately 16.72 nm. The BET surface area of the material was 22.99 $m^2\ g^{-1}$.

In order to understand the formation of the 3D hierarchical twin-spheres of the precursor, the effect of the reaction time on its morphology was investigated carefully. The structural evolution of the precursor is presented in **Figure 5**. It can be clearly observed that 1D nanorods (Figure 5a) could be produced after reacting for 2 h. Accompanying prolonging the reaction time to 3 h, however, nanowire bundles with sheaf-like structures (Figure 5b) could be yielded. The shape of the precursor further changed into flower-like structures (Figure 5c) after increasing the reaction time to 4 h. It was found that 3D hierarchical dumbbell-like structures (Figure 5d) could be obtained after prolonging the reaction time to 5 h. The structure of the precursor finally evolved into 3D hierarchical twin-spheres, as shown in Figure 5e, after reacting for 6 h.

It has been found previously that 1D nanorods can grow into self-assembled, sheaf-like bundles based on a crystal-splitting mechanism.[56–58] Our observations of the effect of time on the morphology of the precursor reveal not only its fast growth nature, but also complex splitting behaviors of the materials. We thus suggest a multistep-splitting mechanism to understand the formation of the 3D hierarchical twin-spheres with urchin-like structures (**Figure 6**a). 1) After the formation

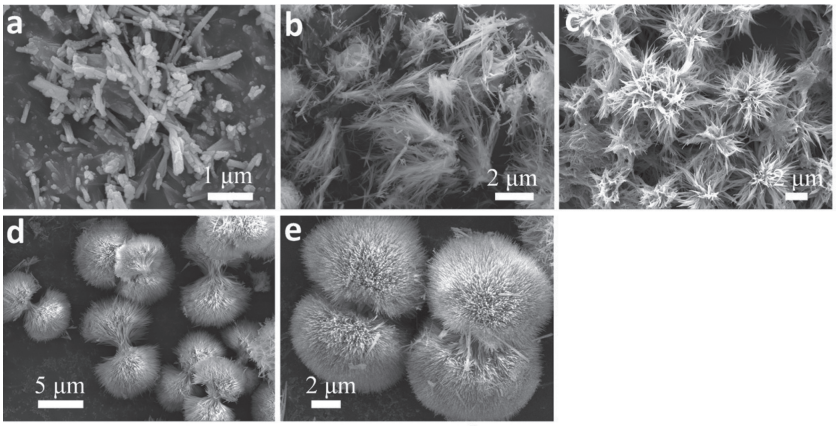

Figure 5. a–e) FE-SEM images of the precursors synthesized at 160 °C for 2 h (a); 3 h (b); 4 h (c); 5 h (d) and 6 h (e).

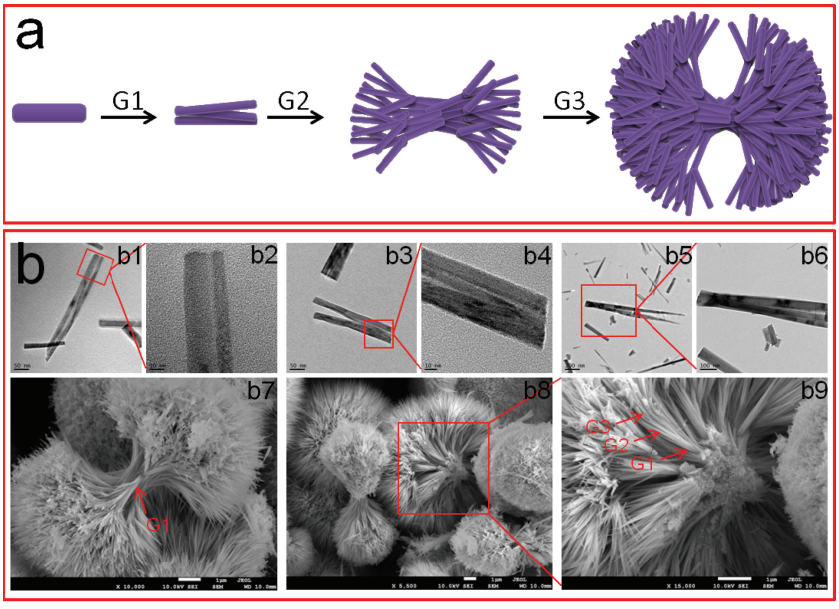

Figure 6. a) Scheme illustrating the multistep-splitting growth mechanism of the precursor with 3D hierarchical structure. b) TEM (b1–b6) and FE-SEM (b7–b9) images of the precusors synthesized based on multistep-splitting growth.

of nuclei in the reaction system, the fast growth of precursor yields nanorods as shown in Figure 5a; 2) due to the subsequent splitting, growth can take place at the two heads of the nanorods, and branched nanorods as shown in Figure 6a(G1) could be produced in the first generation of crystal splitting accompanying the prolonged reaction time. The TEM observations (Figure 6b(b1–b6)) of the precursor, which were collected at the early formation stage of the precursor after reacting for 2 h, clearly indicate that the branches generated from the two ends of the nanorods had already been produced in the first generation of the splitting growth. Sheaf-like bundles of the precursor (Figure 5b) could thus be produced in the reaction after prolonging the reaction time to 3 h. 3) The splitting growth can further occur not only from the seeded nanorods continually, but also from the freshly generated tips of the nanoneedles consisting of the sheaf-like bundles. The nanorods approximately 1.5 μm in length in each generation could split into more than two nanoneedles with smaller diameters. Precursors with a sheaf-like structure could be produced in the first or second-generation of splitting growth (Figure 6a(G2)). 4) Because the growth could take place at the tips of the nanoneedles repeatedly (Figure 6a(G3)), the number of precursor nanoneedles increased explosively after their splitting for three or more generations. Due to the direction of the freshly generated nanoneedles always relating to and definitely deviating from the axis of the 1D seeded nanoneedles, two hemispheres could be produced eventually in the multistep-splitting growth from nanorod seeds, to form the 3D hierarchical dumbbell-like structures, as shown in Figure 5d,e. The multistep-splitting growth could be observed directly in the FE-SEM images of the precursor, as shown in Figure 6b(b7–b9). The red arrows in Figure 6b(b8) and Figure 6b(b9) highlight the first-, second-, and third-generation of the splitting growth (asigned as G1, G2, and G3). It could be found that 3D hierarchical twin-spheres with a dumbbell-like structure could be generated after splitting for more than three generations (Figure 6a(G3) and Figure 6b(b9)).

The crystal splitting is generally associated with fast crystal growth and could be dramatically affected by the reaction parameters, such as the medium and the reactant. It was found that no precursor was yielded in the experiments without adding glucose into the system as a control. The results indicate that glucose also plays an important role in the formation of precursor in the reaction. We therefore investigated the effect of the amount of glucose on the formaion of the 3D hierarchical nanoarchitecture. While we lost the control to some extent in the hierarchical structure of the precursor, the 3D hierarchical dumbbells were yielded after adding 10 times more glucose (0.28 mmol) into the reaction. However, the morphology of the precursor changed dramatically into large spheres with a smooth surface, after adding an excessive amount of glucose (0.56 mmol and 5.6 mmol) into the reaction. It is not clear why there were no 3D hierarchical nanostructures produced after adding more glucose into the reaction. The glucose may act not only as a reactant to generate carbonate groups reacting with Co^{2+} ions to form the precursor (Equation 1), but also as a surfactant to modify the surface of the precursor. The excessive glucose in the system could inhibit the anisotropic growth of precursor along its [100] direction.

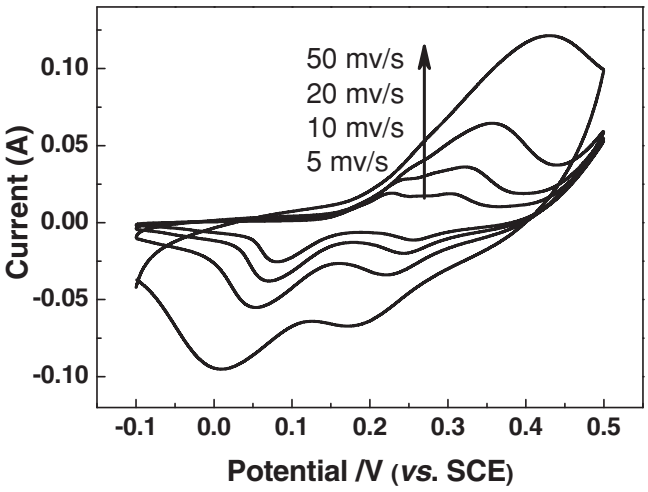

Figure 7. Cyclic voltammograms of the 3D hierarchical Co_3O_4 twin-spheres in KOH electrolyte at various scan rates of 5, 10, 20, and 50 mV s^{-1}.

$$12Co^{2+} + C_6H_{12}O_6 + 7O_2 + 11.32H_2O \rightarrow 12Co(CO_3)_{0.5}(OH) \cdot 0.11H_2O + 2OH^+ \quad (1)$$

Due to the 3D hierarchical nanoarchitectures generally possessing the advantages both of nanostructured and bulk materials, the as-prepared Co_3O_4 twin-spheres could be promising candidates for designing novel devices such as supercapacitors. We thus fabricated supercapacitors using the materials as building blocks to construct electrodes for storing energy. **Figure 7** shows cyclic voltammograms (CVs) of the 3D hierarchical Co_3O_4 twin-spheres recorded at different scan rates between 5 and 50 mV s^{-1} in KOH solution. All of the curves show obvious pseudocapacitance features with a similar linetype.[35,40,42] Two pairs of redox peaks were observed at a scan rate of 5 mV s^{-1}, which correspond to the conversion between different cobalt oxidation states, according to Equation 2 and Equation 3.

$$Co_3O_4 + OH^- + H_2O \Leftrightarrow 3CoOOH + e^- \quad (2)$$

$$CoOOH + OH^- \Leftrightarrow CoO_2 + H_2O + e^- \quad (3)$$

Accompanying the increase of the scan rate, the peak currents were also increased, which suggests the good reversibility of the fast charge-discharge response of the materials.

Figure 8a shows the charge and discharge curves of the pseudocapacitors made with as-prepared materials, measured at different discharge current densities within the potential window of –0.05–0.35 V in KOH solution. The specific capacitances of the materials evaluated from the discharge curves were 781, 754, 700, 670, and 611 F g^{-1} at current densities of 0.5, 1, 2, 4, and 8 A g^{-1}, respectively (Figure 8b). Compared with the specific capacitances of Co_3O_4 nanowires, the capacitance values of the 3D hierarchical Co_3O_4 twin-spheres are much higher.[33,49] They are also comparable to those of supercapacitors constructed with ultralayered Co_3O_4 materials.[37] The excellent performances of the devices can be attributed to the unique 3D hierarchical structure of the materials. The capacitance decrease corresponding to the increase of the discharge current density likely resulted from the increase of the potential drop due to the resistance of the nanoneedles and the relatively insufficient Faradic redox reaction of the active material under higher discharge current densities. Importantly, compared with a specific capacitance of 781 F g^{-1} at 0.5 A g^{-1}, the value of 611 F g^{-1} at 8 A g^{-1} only decreased 21.7% (Figure 8b). Compared with the performance of ultralayered materials,[37,55] the lower fading rate in the capacitance of the novel 3D hierarchical Co_3O_4 twin-spheres at high galvanostatic current density indicates that the materials allowed for the redox reaction taking place rapidly at high current densities, which can be attributed to the high ion permeability in the 3D hierarchical structure.

A long cycle life of supercapacitors is another crucial functionality of the devices, and can determine their practical applications. We further performed a charge/discharge cycling test to examine the long-term cyclability of electrodes made with the 3D hierarchical Co_3O_4 twin-spheres. The galvanostatic charge-discharge curves of the materials, as shown in Figure 8c, indicate that the charge-discharge process of the electrode was highly reversible. Figure 8d shows the cycling performance of the 3D hierarchical Co_3O_4 twin-spheres at a current density of 4 A g^{-1} within the potential window of –0.05–0.35 V. After cycling for 200 times, there was a very small decrease of the capacitance, which could have resulted from the consumption of electrolyte, caused by the irreversible reaction between the electrode materials and electrolyte. The capacitance of the device kept almost constant after that, and retained approximately 97.8% of its maximum value, after cycling 1000 times. The results indicate that these 3D hierarchical Co_3O_4 twin-spheres are promising candidate for designing high-performance supercapacitors.

Typical Nyquist plots of the electrodes made with the 3D hierarchical Co_3O_4 twin-spheres before and after charge-discharge cycling measurements are presented in **Figure 9**. From the point intersecting with the real axis in the range of high frequency, the internal resistances of the 3D hierarchical Co_3O_4 nanoarchitectures were evaluated to be approximately 0.7 Ω and 0.65 Ω, respectively, before and after the charge-discharge cycling measured in an open-circuit condition. The plots measured before and after charge-discharge cycling consisted of semicircles in the high-frequency region and straight lines with slopes of 66.8° and 58.2° in the low-frequency region. The semicircle is related to Faradic reactions. A slope higher than 45° in the electrochemical impedance spectroscopy (EIS) curve suggests that the Warburg resistance is not the determinable factor and the electrode can store charges more efficiently. The results further indicate that the 3D hierarchical Co_3O_4 twin-spheres are excellent electrode materials for fabricating supercapacitors. In addition, the increase of the Warburg resistance after cycling 1000 times can be attributed to the loss of adhesion of some active material blocking the diffusion pathways of ions during the charge-discharge process.

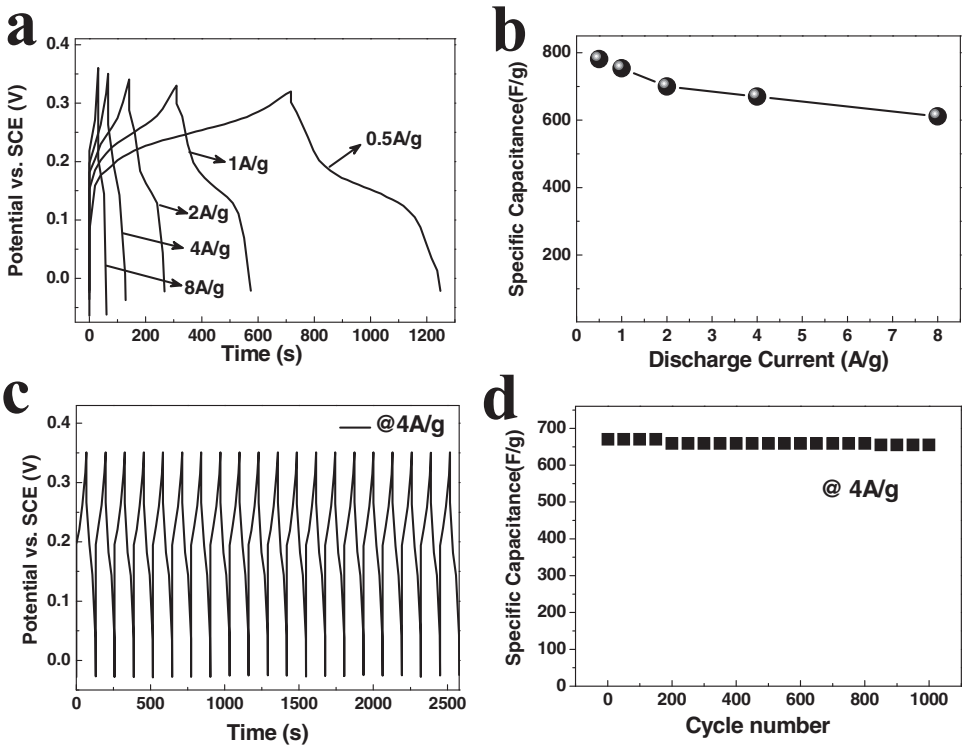

Figure 8. a) The charge-discharge curves of the 3D hierarchical Co_3O_4 twin-spheres measured at different current densities. b) Average specific capacitance of the 3D hierarchical Co_3O_4 twin-spheres at various discharge current densities. c) Galvanostatic charge-discharge curves of the 3D hierarchical Co_3O_4 twin-spheres at a current density of 4 A g^{-1}. d) Average specific capacitance versus cycle number of 3D hierarchical Co_3O_4 twin-spheres at a galvanostatic charge and discharge current density of 4 A g^{-1}.

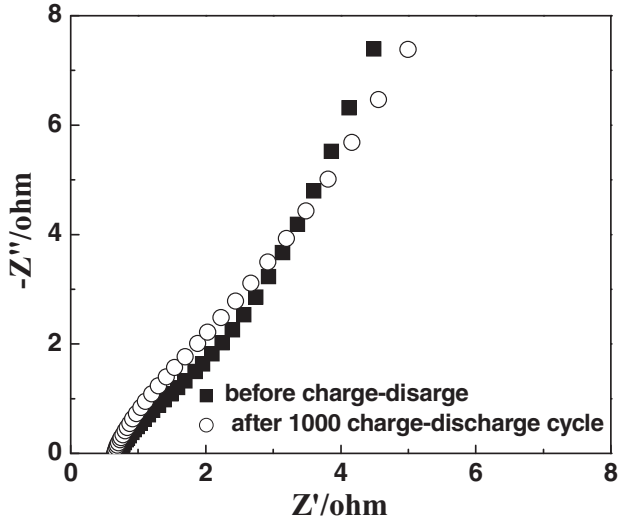

Figure 9. Nyquist plots of the 3D hierarchical Co_3O_4 nanoarchitecture electrode before and after charge-discharge cycling.

3. Conclusions

In summary, 3D nanoarchitectures– hierarchical Co_3O_4 twin-spheres with an urchin-like structure– were synthesized successfully for the first time. It was found that the reaction time and the glucose reactant could dramatically affect the growth of the Co_3O_4 twin-spheres. A multistep-splitting growth mechanism is proposed to understand the formation of the novel 3D hierarchical nanoarchitectures. The materials were further used as building blocks to construct supercapacitors exhibiting high specific capacitance and electrochemical stability at high current densities. The excellent electrochemical performances of the Co_3O_4 materials could be attributed to their unique 3D hierarchical nanostructure, which could significantly increase the work stability of the electrodes, as well as the rate for ion diffusion and electron transportation in the constructed supercapacitors. Based on the multistep-splitting growth proposed, a new pathway can be opened to construct 3D hierarchical nanostructures for advanced electrode materials that are highly desirable in the design of novel devices, such as supercapacitors, Li rechargable batteries and (bio-)chemical sensors with excellent performances.

4. Experimental Section

All of the reagents were analytically pure, and were purchased from the Shanghai Chemical Industrial Co. Ltd. (Shanghai, China); they were used without further purification.

Cobalt nitrate hexahydrate ($Co(NO_3)_2{\cdot}6H_2O$) (1.455 g, 5.00 mmol) was dissolved in deionized water (20 mL) and ethylene glycol ($C_2H_6O_2$) (20 mL) under stirring. The resulting solution was stirred until it became transparent. Subsequently, glucose (0.005 g, 0.028 mmol) was added

into the solution and the mixture was stirred for another 30 min. The whole mixture was then transferred into a polytetrafluoroethylene (PTFE) (Teflon)-lined autoclave and maintained at 160 °C for 16 h. After cooling to room temperature naturally, the precipitates were collected by centrifugation, thoroughly washed with deionized water and ethanol 5 times each, and dried in an oven at 70 °C for 12 h to get red powders of the precursor. Finally, the samples were calcined in a muffle furnace at 300 °C for 2 h in air, and then cooled down to room temperature naturally. The as-prepared black powders with a yield of 91% were collected for characterization and application.

The as-prepared precursors and products were characterized by powder XRD using a D/max 2550V X-ray diffractometer (Rigaku, Tokyo, Japan) with monochromatized Cu K_α (λ = 1.54056 Å; scanning rate: 0.02° s^{-1} in the range of 10–70°) incident radiation and by Fourier transform IR (FTIR) spectroscopy (Nicolet Co., USA). The morphologies and the structures of all the products were analyzed by FE-SEM (JSM-7001F), TEM and SAED (JEM-2100 operated at 200 kV).

The electrochemical studies were carried out in a three-electrode system with a KOH electrolyte solution (6 mol L^{-1}). The freshly prepared Co_3O_4 twin-spheres on nickel meshes, a platinum electrode, and a saturated calomel electrode (SCE) were used as the working electrode, counter electrode, and reference electrode, respectively. The working electrode was composed of active Co_3O_4 materials (80 wt%), conductive material (acetylene black, ATB, 10 wt%) and binder (PTFE, 10 wt%). The mixture was first coated onto the surface of a piece of nickel foam sheet (1 cm × 1 cm), and then dried at 100 °C for 12 h. The sheets with active materials were finally pressed under 10 MPa to obtain the working electrode. The cyclic voltammogram (CV) and electrochemical impedance spectroscopy (EIS) were measured with a CHI 660D electrochemical workstation. CV tests were done between –0.1 and 0.5 V (vs. saturated calomel electrode (SCE)) at scan rates of 5, 10, 20, and 50 mV s^{-1}, respectively, and the EIS measurements were carried out in the frequency range from 0.01 Hz to 100 kHz at an open-circuit potential with an ac perturbation of 5 mV. Galvanostatic charge/discharge cycle tests were performed on a CT2001A LAND Cell test system. The specific capacitance of the supercapacitors could be evaluated from the charge/discharge test together with the following equation:

$$C_m = I\Delta t/m\Delta V \quad (4)$$

where C_m is the specific capacitance of the capacitor (F g^{-1}), I is the current of charge/discharge, and Δt is the discharging time period in seconds for the potential change ΔV, in volts; m is the mass load of the active material. All of the electrochemical measurements were carried out at room temperature.

Acknowledgements

The authors are grateful to the financial support from the National Science Foundation of China (NSFC. 21071130), the Outstanding Scholar Program of Henan Province (114200510012), and the State Key Programs for Science and Technology of Henan Province (92102310334 and 112102210239).

Received: February 22, 2012
Revised: April 17, 2012
Published online: June 11, 2012

[1] C. Liu, F. Li, L. P. Ma, H. M. Cheng, *Adv. Mater.* **2010**, *22*, E28.
[2] P. J. Hall, M. Mirzaeian, S. I. Fletcher, F. B. Sillars, A. J. R. Rennie, G. O. Shitta-Bey, G. Wilson, A. Cruden, R. Carter, *Energy Environ. Sci.* **2010**, *3*, 1238.
[3] D. R. Rolison, J. W. Long, J. C. Lytle, A. E. Fischer, C. P. Rhodes, T. M. McEvoy, M. E. Bourg, A. M. Lubers, *Chem. Soc. Rev.* **2009**, *38*, 226.
[4] J. R. Miller, P. Simon, *Science* **2008**, *321*, 651.
[5] P. Simon, Y. Gogotsi, *Nat. Mater.* **2008**, *7*, 845.
[6] A. S. Arico, P. Bruce, B. Scrosati, J. M. Tarascon, W. Van Schalkwijk, *Nat. Mater.* **2005**, *4*, 366.
[7] Z. J. Fan, J. Yan, T. Wei, L. Zhi, G. Ning, T. Li, F. Wei, *Adv. Funct. Mater.* **2011**, *21*, 2366.
[8] Y. Y. Liang, M. G. Schwab, L. Zhi, E. Mugnaioli, U. Kolb, X. Feng, K. Müllen, *J. Am. Chem. Soc.* **2010**, *132*, 15030.
[9] J. Chmiola, C. Largeot, P. L. Taberna, P. Simon, Y. Gogotsi, *Science* **2010**, *328*, 480.
[10] K. Xie, X. Qin, X. Wang, Y. Wang, H. Tao, Q. Wu, L. Yang, Z. Hu, *Adv. Mater.* **2012**, *24*, 347.
[11] S. Chen, J. Zhu, X. Wu, Q. Han, X. Wang, *ACS Nano* **2010**, *4*, 2822.
[12] X. Wang, X.-L. Wu, Y.-G. Guo, Y. Zhong, X. Cao, Y. Ma, J. Yao, *Adv. Funct. Mater.* **2010**, *20*, 1680.
[13] D. N. Futaba, K. Hata, T. Yamada, T. Hiraoka, Y. Hayamizu, Y. Kakudate, O. Tanaike, H. Hatori, M. Yumura, S. Iijima, *Nat. Mater.* **2006**, *5*, 987.
[14] M. S. Song, K. M. Lee, Y. R. Lee, I. Y. Kim, T. W. Kim, J. L. Gunjakar, S.-J. Hwang, *J. Phys. Chem. C* **2010**, *114*, 22134.
[15] T. Brezesinski, J. Wang, S. H. Tolbert, B. Dunn, *Nat. Mater.* **2010**, *9*, 146.
[16] J. P. Liu, J. Jiang, C. Cheng, H. Li, J. Zhang, H. Gong, H. J. Fan, *Adv. Mater.* **2011**, *23*, 2076.
[17] L. Q. Mai, F. Yang, Y.-L. Zhao, X. Xu, L. Xu, Y.-Z. Luo, *Nat. Commun.* **2011**, *2*, 1.
[18] H. L. Wang, Q. M. Gao, L. Jiang, *Small* **2011**, *7*, 2454.
[19] J. W. Xiao, S. H. Yang, *RSC Adv.* **2011**, *1*, 588.
[20] C. C. Hu, K. H. Chang, M. C. Lin, Y. T. Wu, *Nano Lett.* **2006**, *6*, 2690.
[21] W. Sugimoto, H. Iwata, Y. Yasunaga, Y. Murakami, Y. Takasu, *Angew. Chem. Int. Ed.* **2003**, *42*, 4092.
[22] M. W. Xu, F. Wang, M. S. Zhao, S. Yang, X. P. Song, *Electrochim. Acta* **2011**, *56*, 4876.
[23] J. P. Zheng, P. J. Cygan, T. R. Jow, *J. Electrochem. Soc.* **1995**, *142*, 2699.
[24] D. W. Wang, Q. H. Wang, T. M. Wang, *Nanotechnology* **2011**, *22*, 135604.
[25] W. Chen, R. B. Rakhi, L. Hu, X. Xie, Y. Cui, H. N. Alshareef, *Nano Lett.* **2011**, *11*, 5165.
[26] W. B. Yan, T. Ayvazian, J. Kim, Y. Liu, K. C. Donavan, W. Xing, Y. Yang, J. C. Hemminger, R. M. Penner, *ACS Nano* **2011**, *5*, 8275.
[27] L. B. Hu, W. Chen, X. Xie, N. Liu, Y. Yang, H. Wu, Y. Yao, M. Pasta, H. N. Alshareef, Y. Cui, *ACS Nano* **2011**, *5*, 8904.
[28] C. Jo, I. Hwang, J. Lee, C. W. Lee, S. Yoon, *J. Phys. Chem. C* **2011**, *115*, 11880.
[29] C. Z. Yuan, L. Yang, L. Hou, L. Shen, F. Zhang, D. Li, X. Zhang, *J. Mater. Chem.* **2011**, *21*, 18183.
[30] Y. Q. Fan, H. Shao, J. Wang, L. Liu, J. Zhang, C. Cao, *Chem. Commun.* **2011**, 3469.
[31] T. T. Zhu, Y. F. Liu, Z. H. Hu, C. C. Wang, Z. B. Wen, *J. Mater. Sci.: Mater. Electron.* **2011**, *22*, 1649.
[32] F. Zhang, L. Hao, L. J. Zhang, X. G. Zhang, *Int. J. Electrochem. Sci.* **2011**, *6*, 2943.
[33] X. H. Xia, J. Tu, Y. Mai, X. Wang, C. Gu, X. Zhao, *J. Mater. Chem.* **2011**, *21*, 9319.
[34] J. B. Wu, Y. Lin, X. H. Xia, J. Y. Xu, Q. Y. Shi, *Electrochim. Acta.* **2011**, *56*, 7163.
[35] L. Wang, X. H. Liu, X. Wang, X. J. Yang, L. D. Lu, *J. Mater. Sci.: Mater. Electron.* **2011**, *22*, 601.
[36] D. W. Wang, Q. H. Wang, T. M. Wang, *Inorg. Chem.* **2011**, *50*, 6482.
[37] S. K. Meher, G. R. Rao, *J. Phys. Chem. C* **2011**, *115*, 15646.
[38] S. K. Meher, G. R. Rao, *J. Phys. Chem. C* **2011**, *115*, 25543.

[39] Y. H. Li, K. L. Huang, Z. F. Yao, S. Q. Liu, X. X. Qing, *Electrochim. Acta* **2011**, *56*, 2140.
[40] Y. H. Li, K. L. Huang, S. Q. Liu, Z. F. Yao, S. X. Zhuang, *J. Solid State Electrochem.* **2011**, *15*, 587.
[41] S. G. Kandalkar, H. M. Lee, H. Chae, C. K. Kim, *Mater. Res. Bull.* **2011**, *46*, 48.
[42] L. R. Hou, C. Yuan, L. Yan, L. Shen, F. Zhang, X. Zhang, *RSC Adv.* **2011**, *1*, 1521.
[43] Y. Liu, W. Zhao, X. Zhang, *Electrochim. Acta* **2008**, *53*, 3296.
[44] T. Zhu, J. S. Chen, X. W. Lou, *J. Mater. Chem.* **2010**, *20*, 7015.
[45] J. A. Xu, L. Gao, J. Y. Cao, W. C. Wang, Z. D. Chen, *Electrochim. Acta* **2010**, *56*, 732.
[46] L. Wang, X. H. Liu, X. Wang, X. J. Yang, L. D. Lu, *Curr. Appl. Phys.* **2010**, *10*, 1422.
[47] J. K. Lee, G. P. Kim, K. H. Kim, I. K. Song, S. H. Baeck, *J. Nanosci. Nanotechnol.* **2010**, *10*, 3676.
[48] S. G. Kandalkar, D. S. Dhawale, C. K. Kim, C. D. Lokhande, *Synth. Met.* **2010**, *160*, 1299.
[49] Y. Y. Gao, S. L. Chen, D. X. Cao, G. L. Wang, J. L. Yin, *J. Power Sources* **2010**, *195*, 1757.
[50] M. B. Zheng, J. Cao, S. Liao, J. Liu, H. Chen, Y. Zhao, W. Dai, G. Ji, J. Cao, J. Tao, *J. Phys. Chem. C* **2009**, *113*, 3887.
[51] T. Y. Wei, C. H. Chen, K. H. Chang, S. Y. Lu, C. C. Hu, *Chem. Mater.* **2009**, *21*, 3228.
[52] S. G. Kandalkar, J. L. Gunjakar, C. D. Lokhande, *Appl. Surf. Sci.* **2008**, *254*, 5540.
[53] V. R. Shinde, S. B. Mahadik, T. P. Gujar, C. D. Lokhande, *Appl. Surf. Sci.* **2006**, *252*, 7487.
[54] H. T. Wang, L. Zhang, X. Tan, C. M. B. Holt, B. Zahiri, B. C. Olsen, D. Mitlin, *J. Phys. Chem. C* **2011**, *115*, 17599.
[55] S. L. Xiong, C. Z. Yuan, M. F. Zhang, B. J. Xi, Y. T. Qian, *Chem. Eur. J.* **2009**, *15*, 5320.
[56] J. Tang, A. P. Alivisatos, *Nano Lett.* **2006**, *6*, 2701.
[57] X. F. Shen, X. P. Yan, *Angew. Chem. Int. Ed.* **2007**, *46*, 7659.
[58] L. S. Li, N. Sun, Y. Huang, Y. Qin, N. Zhao, J. Gao, M. Li, H. Zhou, L. Qi, *Adv. Funct. Mater.* **2008**, *18*, 1194.